CHEMISTRY OF MATERIALS

Article

pubs.acs.org/cm

Seed Size-Dependent Formation of Fe_3O_4/MnO Hybrid Nanocrystals: Selective, Magnetically Recyclable Catalyst Systems

Kyung Sig Lee,[†] Rahman Md Anisur,[†] Ki Woong Kim,[†] Won Sun Kim,[†] Tae-Joon Park,[‡] Eun Joo Kang,[†] and In Su Lee*,[‡]

[†]Department of Applied Chemistry, Kyung Hee University, Gyeonggi-do 446-701, Korea

[‡]Department of Chemistry, Pohang University of Science and Technology (POSTECH), Pohang 790-784, Korea

ABSTRACT: A family of Fe_3O_4/MnO hybrid nanocrystals differing in heterojunction structure and number of MnO domains were synthesized through the seed-mediated growth process of MnO at the surface of Fe_3O_4 nanocrystal. In this process, the resulting heterostructures, including core/shell, dumbbell-like, and flowerlike structures, were found to be largely influenced by the size of initially injected Fe_3O_4 seeds. The further transformation of Fe_3O_4/MnO heterodimer through a nanoscale etching process within silica nanosphere generated the nanoreactor framework composed of a superparamagnetic Fe_3O_4 nanocrystal, a functionalized cavity with a catalytically active Mn_3O_4 layer, and a porous silica shell. The newly developed nanoreactor successfully catalyzed the cyanosilylation reaction of aromatic aldehydes in a size selective manner and could be recovered magnetically and reused without loss of catalytic activity even after ten successive cycles.

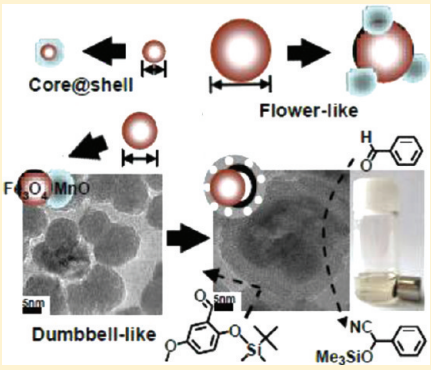

KEYWORDS: *hybrid nanocrystal, manganese, iron, nanocatalyst, recyclable catalyst*

■ INTRODUCTION

The synthesis and fabrication of hybrid nanocrystals containing two or more chemically and/or functionally different species is an important achievement in nanochemistry.[1−3] The most studied hybrid nanocrystals have been of the core/shell structural type, in which a nanocrystalline core is encased in a shell composed of a different material. In recent years, phase-segregated heterostructures, in which two or more inorganic domains are joined through a small interfacial area, have attracted increased attention. In particular, heterodimers composed of magnetic components including M/Fe_3O_4 (M = Au, Ag, Ni, Pd, Pt), CdS/FePt, CdSe/Fe_3O_4, and γ-Fe_2O_3/metal sulfides have received significant scrutiny due to their novel properties and potential applications that cannot be achieved solely with single component nanocrystals.[4−11] In this context, this study initially intended to integrate superparamagnetic iron oxide and Lewis acidic manganese oxide nanoparticles into a single hybrid nanocrystal. In the course of synthesizing hybrid nanocrystals through the seed-mediated growth method, a family of Fe_3O_4/MnO hybrid nanocrystals differing in heterojunction structure and number of MnO domains were produced. Importantly, in this process, the hybrid nanocrystal morphology type, core/shell, heterodimer, or flowerlike nanocrystal, was found to be largely influenced by the size of the initially injected seed nanocrystal.[12,13] In addition to providing fundamental knowledge, this finding offers a novel basis for the fabrication of nanoreactor systems. The newly synthesized Fe_3O_4/MnO heterodimer could be further transformed into a heterodimer consisting of solid Fe_3O_4 and hollow Mn_3O_4 grains through a recently developed nanoscale etching process within silica nanospheres.[14−17] The employment of such a transformation generated the hollow nanoreactor framework for a selective, magnetically recyclable catalyst composed of a superparamagnetic Fe_3O_4 nanocrystal, a functionalized cavity with a catalytically active Mn_3O_4 layer, and a porous silica shell.

We report our findings on the formation of various Fe_3O_4/MnO hybrid nanocrystals through the seed-mediated growth process and the influence of seed size on the resulting heterostructures. We also report the successful employment of Fe_3O_4/MnO hybrid nanocrystals for the fabrication of a nanoreactor system and which selectively catalyzed the cyanosilylation reaction of aromatic aldehydes and could be recovered via magnetic separation and reused in multiple iterations.

■ RESULTS AND DISCUSSION

Synthesis of Fe_3O_4/MnO Hybrid NCs with Various Heterojunction Structures. For the preparation of Fe_3O_4/MnO hybrid nanocrystals, we adopted the previously reported seed-mediated growth method. First, 5, 11, and 21 nm sized Fe_3O_4 nanocrystals were prepared via thermal decomposition of an Fe(III)-oleate complex. The seed Fe_3O_4 nanocrystals were injected into a trioctylamine solution of $Mn(CH_3CO_2)_2$ and oleic acid to initiate the growth process.[18,19] In all of the syntheses, the initial concentration of $Mn(CH_3CO_2)_2$ was

Received: September 15, 2011
Revised: January 27, 2012
Published: February 9, 2012

constant (0.61 mM). The reaction temperature was then slowly increased to 320 °C, thereby allowing nucleation and growth of MnO at the Fe_3O_4 surface to occur. The reaction nanoparticles were isolated by addition of excess ethanol, followed by centrifugation. The shapes of the resulting Fe_3O_4/MnO hybrid nanocrystals, observed using transmission electron microscopy (TEM), were found to vary depending on the size of the initially injected Fe_3O_4 nanocrystal seeds (Scheme 1). The

Scheme 1. Seed Size-Dependent Formation of Fe_3O_4/MnO Hybrid Nanocrystals

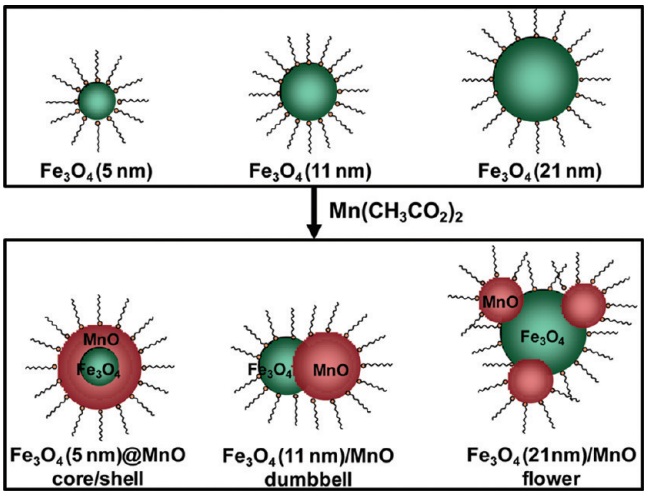

reaction utilizing 5 nm sized Fe_3O_4 seed nanoparticles provided uniform growth of a 3 nm thick MnO shell layer around the Fe_3O_4 seed core to produce a spherical core/shell structured Fe_3O_4(5 nm)/MnO NP (Figure 1a). The formation of a core/shell structure is analogous with structures previously observed from the synthesis of MFe_2O_4@MnO (M = Co, Zn) nanocrystals using 5-nm-sized MFe_2O_4 seeds.[19] On the other hand, in the reaction with 11 nm sized Fe_3O_4 seed nanocrystals, MnO was found to nucleate only at a single surface site on the Fe_3O_4 seed. Further MnO growth on the nuclei resulted in the formation of a dumbbell-shaped heterodimer, Fe_3O_4(11 nm)/MnO NP, in which 16 nm sized MnO and 11 nm sized Fe_3O_4 grains were joined through a small interfacial area (Figure 1b). The fringe distances, measured from a high resolution TEM (HRTEM) image, were 2.22 and 2.42 Å for the two types of grains, which are well-matched with the known lattice distances for MnO and Fe_3O_4 phases, respectively. Based on the energy dispersive X-ray spectroscopic (EDS) map, these two grain types were identified as being composed of Mn and Fe (insets in Figure 1b,c). The X-ray diffraction (XRD) pattern also confirmed the formation of a MnO phase that preserved the crystalline phase of the initially injected Fe_3O_4 seed nanocrystals (Figure 2). When 21 nm sized Fe_3O_4 nanocrystals were injected into the reaction suspension, MnO nucleation occurred at several sites on the Fe_3O_4 surface. The simultaneous growth of multiple MnO grains on a single seed nanocrystal generated a flowerike heterostructure, Fe_3O_4(21 nm)/MnO, with several MnO petals of a 16 nm average size arranged on a central Fe_3O_4 particle (Figure 1c).

Although an exact mechanism to explain the formation of these differing nanoparticle composites requires further research, the generation of the core/shell type structure only from the 5 nm sized Fe_3O_4 seed can be rationalized based on

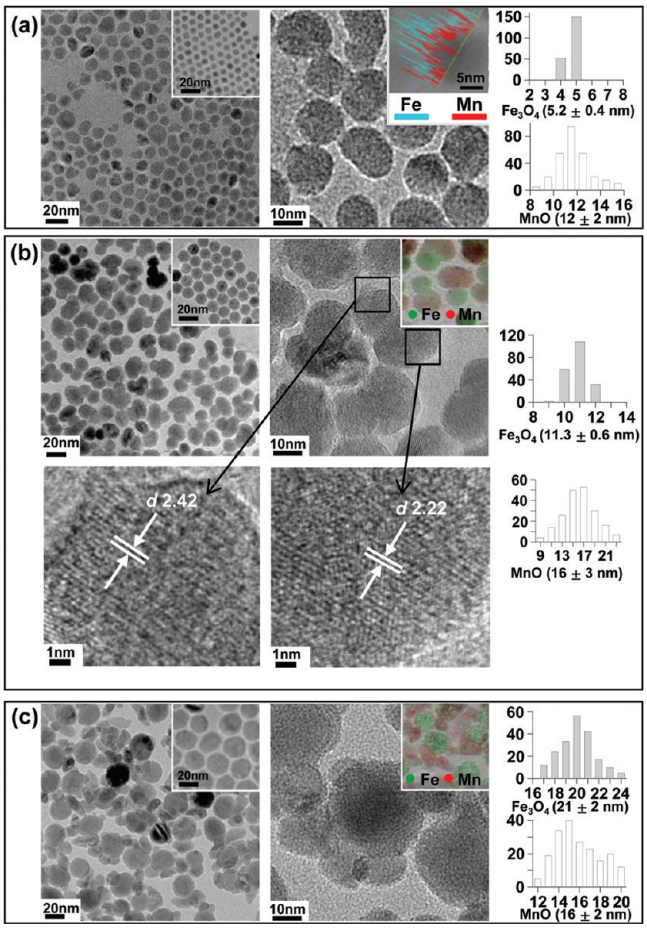

Figure 1. TEM and HRTEM images of (a) core/shell type Fe_3O_4(5 nm)/MnO, (b) dumbbell-shaped Fe_3O_4(11 nm)/MnO, and (c) flower-shaped Fe_3O_4(21 nm)/MnO NCs and histograms showing the size distribution of the Fe_3O_4 and MnO grains. Insets in the left images: TEM images of the Fe_3O_4 nanocrystals used as seeds. Insets in the right images: STEM line profiling and EDS maps showing the distribution of Fe and Mn elements.

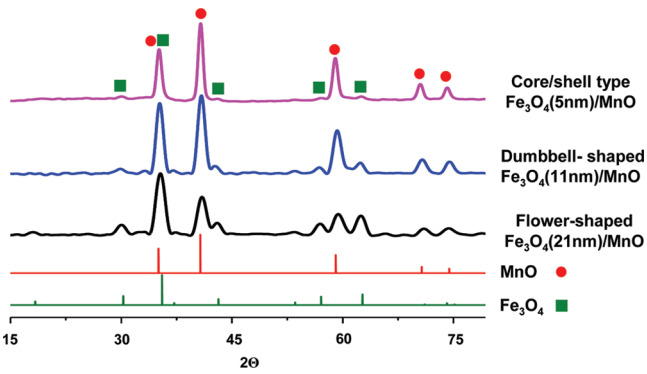

Figure 2. XRD patterns of core/shell type Fe_3O_4(5 nm)/MnO, dumbbell-shaped Fe_3O_4(11 nm)/MnO, and flower-shaped Fe_3O_4(21 nm)/MnO NCs. Peaks corresponding to Fe_3O_4 and MnO are marked with green squares and red circles, respectively. The lines below show the position of the reflections corresponding to cubic MnO phase (JCPDS Card No. 07−0230) and the tetragonal Fe_3O_4 phase (JCPDS Card No. 88−0315).

the higher surface chemical potential of the smaller nanocrystals with a high radius of curvature.[20,21] Because the surfaces of 5 nm sized nanocrystals have a high degree of reactivity,

nucleation and growth of the secondary MnO phase is allowed all over the surface, leading to development of a spherical shell around the Fe_3O_4 core. This is also consistent with the previous observation on the preferential growth of the secondary grain onto the high-curvature surface and the lower formation temperature of the shell around the smaller nanocrystal.[22,23] In contrast, for larger nanocrystals with a relatively stable surface, growth of the secondary phase occurs only at special sites, which can facilitate nucleation and/or allow better accommodation of an interfacial system.[24] Therefore, in the cases of 11 and 21 nm sized seed nanocrystals, the number of exposed defects or facets with high reactivity becomes highly influential in determining the number of phase-segregated MnO grains.[25,26]

Synthesis of Nanoreactor Framework from the Fe_3O_4/MnO Heterodimer NC. Concerning prospective applications of these newly synthesized hybrid nanocrystals, the Fe_3O_4/MnO heterodimer NC was further developed as a nanoreactor to function as a selective and magnetically recyclable catalyst.[27−33] The strategy used to fabricate the nanoreactor from the heterodimer NC is illustrated in Scheme 2. In this

Scheme 2. Fabrication of the Nanoreactor, Fe_3O_4/HMON@*h*-SiO_2, from the Fe_3O_4/MnO Heterodimer NC

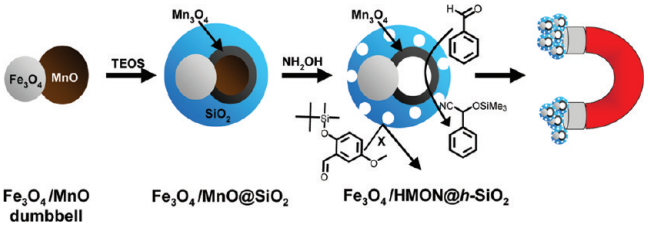

strategy, the MnO phase was selectively removed from the heterodimer NC, generating a Fe_3O_4/hollow Mn_3O_4 heterodimer which combines magnetically controllable flocculation and dispersion properties with the Lewis acid properties of each grain. Fe_3O_4/MnO heterodimer nanocrystals were synthesized by growing 30 nm sized MnO grains on 11 nm sized Fe_3O_4 nanocrystals, which were then encapsulated within a silica shell using a modified emulsion technique. The silica nanosphere-encased Fe_3O_4/MnO heterodimer, Fe_3O_4/MnO@SiO_2, was treated with a 1 M NH_2OH solution in a procedure similar to that previously applied to the synthesis of a hollow Mn_3O_4 nanoshell within a silica nanosphere.[17] TEM, HRTEM, and SEM analyses of nanospheres isolated after a 24 h reaction showed that the MnO grains had been removed, leaving a spherical silica shell with catalytically functionalized cavity by a thin, 4.6-nm-thick Mn_3O_4 layer, whereas the Fe_3O_4 grains maintained their original 11 nm size (Figures 3 and 4). The XRD patterns of the spheres also revealed a significant decrease in the MnO fraction, indicating its preferential dissolution (Figure 3c). MnO dissolution was accompanied by partial etching of the silica shell, resulting in the formation of a hollow nanosphere, Fe_3O_4/HMON@*h*-SiO_2, in which the nanocrystalline Fe_3O_4 particle with superparamagnetic properties and a cavity functionalized with a catalytically active Mn_3O_4 layer were coated by a porous silica shell. The pore size distribution centered at 1 nm, which was derived by using HK model based on the nitrogen adsorption/desorption isotherm, also supports the formation of nanopores at the silica shell (Figure 3e). BET surface was measured to be 73 m^2 g^{-1}. Magnetic measurements

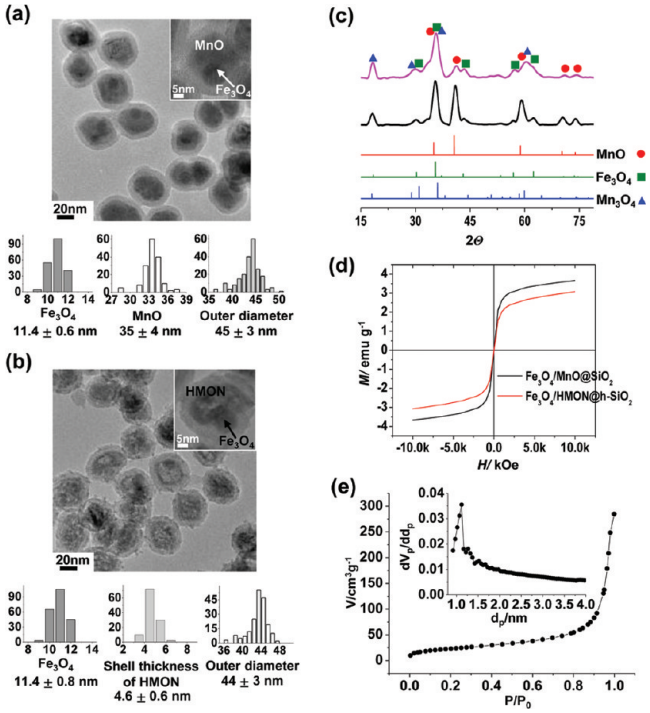

Figure 3. TEM images of (a) Fe_3O_4/MnO@SiO_2 and (b) Fe_3O_4/HMON@*h*-SiO_2 nanospheres. Histograms show the size distribution of the silica sphere and Fe_3O_4 and MnO grains and shell thickness of HMON. Inset: HRTEM images. (c) XRD patterns of Fe_3O_4/MnO@SiO_2 (black line) and Fe_3O_4/HMON@*h*-SiO_2 spheres (magenta line). Peaks corresponding to Fe_3O_4, MnO, and Mn_3O_4 phases are marked with green squares, red circles, and blue triangles, respectively. The lines below show the position of the reflections corresponding to the tetragonal Fe_3O_4 phase (JCPDS Card No. 88−0315), the cubic MnO phase (JCPDS Card No. 07−0230), and the tetragonal Mn_3O_4 phase (JCPDS Card No. 24−0734). (d) Field-dependent magnetization curves at 293 K, showing superparamagnetic characteristics of Fe_3O_4/MnO@SiO_2 and Fe_3O_4/HMON@*h*-SiO_2. (e) N_2 sorption isotherm and pore size distribution (inset) of Fe_3O_4/HMON@*h*-SiO2 derived by using HK model.

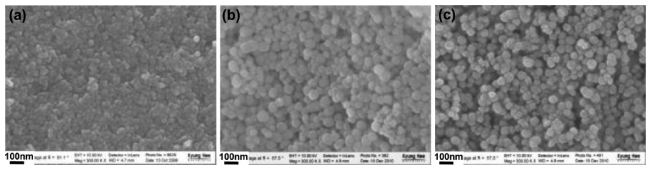

Figure 4. Scanning electron microscopy (SEM) images of the (a) dumbbell-shaped Fe_3O_4(11 nm)/MnO NC and (b) Fe_3O_4/MnO@SiO_2 and (c) Fe_3O_4/HMON@*h*-SiO_2 nanospheres.

show that the Fe_3O_4/HMON@*h*-SiO_2 had a saturated magnetization value of 3.08 emu/g and superparamagnetic behavior at 298 K (Figure 3d). By integrating the properties of each component, it was concluded that the Fe_3O_4/HMON@*h*-SiO_2 could act as a nanoreactor with substrate size selectivity that could be isolated magnetically and recycled.

Evaluation of Catalytic Performance of the Nanoreactor Framework. To evaluate the effectiveness of Fe_3O_4/HMON@*h*-SiO_2 as a selective and recyclable catalyst, it was examined in the cyanosilylation reaction of carbonyl substrates, a reaction facilitated by Lewis acid catalysis. Benzaldehyde (**1a**) was used to optimize suitable conditions, and the reaction treated with cyanotrimethylsilane (1.5 equiv.) and 8 mol %

Table 1. Cyanosilylation of Aryl Aldehydes with Fe_3O_4/HMON@*h*-SiO_2 Catalyst[a]

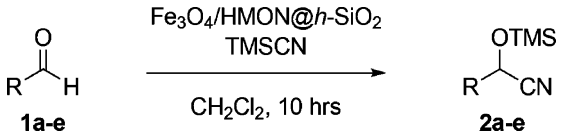

R	product	yield (%)[b]	vol. (Å^3)[c]
phenyl (**1a**)	**2a**	99	85
biphenyl (**1b**)	**2b**	90	145
1-naphthyl (**1c**)	**2c**	70	121
9-antracenyl (**1d**)	**2d**	49	157
2-tert-butyldimethylsiloxy-5-methoxyphenyl (**1e**)	**2e**	8	250
phenyl (**1a**) (10th run)[d]	**2a**	99	
phenyl (**1a**)[e]	**2a**	87	
phenyl (**1a**) (5th run)[d,e]	**2a**	81	

[a]Conditions: aldehyde (0.5 mmol), TMSCN (cyanotrimethylsilane, 0.75 mmol), catalyst (8 mol %, 0.040 mmol, based on Mn contents), CH_2Cl_2 (0.25 M), under N_2. [b]Determined by ^{1}H NMR based on the carbonyl substrate. [c]Molecular volume of aryl aldehydes. [d]The recovered catalyst was used in iterative cycles. [e]Reaction with 4 mol % of catalyst

Fe_3O_4/HMON@*h*-SiO_2 resulted in the cyanohydrin trimethylsilyl ether formation in quantitative yield. In the ^{1}H NMR spectrum to check the conversion yield, the peak at 10.02 ppm (PhC*H*O) disappeared completely and a new peak at 5.50 ppm (PhC*H*CN(OTMS)) was observed. Compared with that of benzaldehyde, the same reaction performed with 1-naphthaldehyde (**1c**) and 9-anthraldehyde (**1d**) afforded the corresponding cyanohydrins in much lower yield of 70 and 50% yields, respectively. In particular, the reaction of 2-tert-butyldimethylsiloxy-5-methoxyphenyl carboxaldehyde (**1e**) reached only 8% yield, representing a significant size-selective reaction in a porous nanoreactor (Table 1).[17,34,35] Molecular volume of aryl aldehydes also shows good correlation with the conversion yield, leading us to theorize that size of the substrates acts as a crucial variable for determining the progress of Fe_3O_4/HMON@*h*-SiO_2-catalyzed cyanosilylation reactions by influencing the diffusion rate through the pores of the silica shell. The reaction with biphenyl carboxaldehyde, affording relatively higher yield than expected correlation, can be understood that a narrow, rod-shaped aldehyde could diffuse rapidly by comparison with others of similar size. The control experiment to check the reactivity of **1e** toward the cyanosilylation reaction was performed with Ti(O^{i}Pr)$_4$ catalyst, and resulted in 98% yield.

After the reaction with benzaldehyde was complete, the Fe_3O_4/HMON@*h*-SiO_2 catalyst was magnetically separated from the product and was reused in consecutive reactions to illustrate its recyclability. When a small magnet was placed on the side of the reaction vessel, the catalyst was primarily concentrated in close proximity to the magnet within 30 min. Decantation of the product solution followed by nanoparticulate washing with CH_2Cl_2 allowed the catalyst to be successfully isolated with no significant loss of material (Figure 5). The recovered catalyst was then subsequently reused in ten further iterative cycles, furnishing the cyanosilylation product with over 95% conversion in each cycle (Table 1). The recycling experiments with 4 mol % of Fe_3O_4/HMON@*h*-SiO_2 catalyst also showed reproducible yield of 81% in five iterative reactions, demonstrating the excellent recyclability of the Fe_3O_4/HMON@*h*-SiO_2. Inductively coupled plasma atomic emission spectroscopy (ICP-AES) analyses of the reaction solutions magnetically separated from the catalyst after each run indicated no loss of catalyst or any leaching of Mn or Fe ions from the catalyst. TEM images of the recovered catalyst also confirmed the preservation of the initial size and structure of the Fe_3O_4/**HMON@***h*-SiO_2 even after ten reaction cycles (Figure 6).

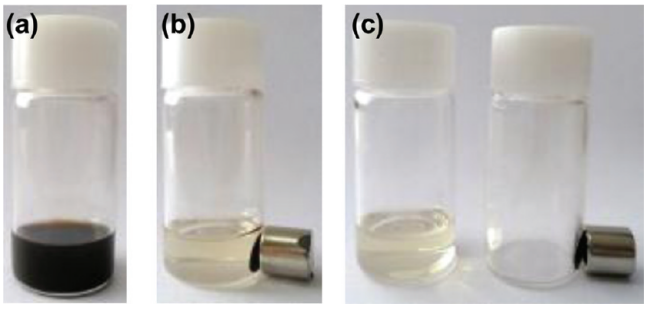

Figure 5. Pictures of the product suspensions (a) before and (b) 10 min after placing a magnet and (c) the decanted product solution (left vial) and the remained Fe_3O_4/HMON@*h*-SiO_2 catalyst (right vial).

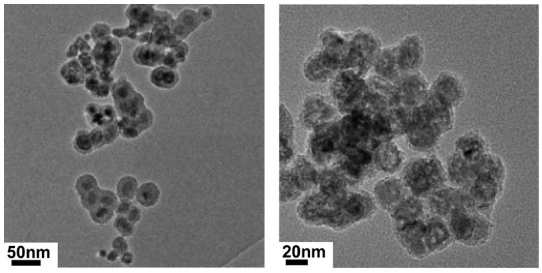

Figure 6. TEM images of the Fe_3O_4/HMON@*h*-SiO_2 catalyst recovered after ten consecutive reactions.

■ EXPERIMENTAL SECTION

General Considerations. All reagents, including $FeCl_3$ (Aldrich), Sodium Oleate (TCI), Oleic acid (Aldrich), Mn(CH_3CO_2)$_2$ (Aldrich), 1-octadecene (Aldrich), hydroxylamine (Aldrich), cyclohexane, NH_4OH (Samchun chem.), tetraethylorthosilicate (Acros), and Igepal CO-520 (Acros), were used as purchased without any further purification. The transmission electron microscopy (TEM) analyses were conducted with a JEOL JEM-2010. Scanning tunneling microscopy (SEM) was carried out with a LEO SUPRA 55 (Carl Zeiss, Germany). The magnetic properties of the nanoparticles were

measured using a superconducting quantum interference device (SQUID) magnetometer (Quantum Design, MPMS5XL) equipped with a 5 T superconducting magnet. The X-ray diffraction patterns were obtained using an X-ray Diffractometer (18 kW) (Mac Science, Japan). The nitrogen adsorption and desorption isotherms were measured at 77 K using a BELSORP-max (BEL Japan) gas adsorption analyzer after the pretreatment at 120 °C in vacuo for 12 h. The ^{1}H NMR spectra were recorded with a Jeol 300 MHz spectrometer and referenced to $CDCl_3$.

Synthesis of Fe_3O_4/MnO Hybrid Nanocrystals. The Fe_3O_4 nanocrystals with sizes of 5, 11, and 21 nm were prepared through the previously reported procedure including the thermal decomposition of Fe-oleic acid complexes at high temperature.[36] Twenty milligrams of powder of Fe_3O_4 nanocrystals, 150 mg of Mn-$(CH_3CO_2)_2$, and 1.28 mg of oleic acid were mixed in 20 mL of trioctylamine solvent. The mixture suspension was slowly heated up to 320 °C. The reaction mixture was maintained at this temperature for 1 h and then cooled to room temperature. Fifteen ml of hexane and 20 mL of acetone were injected into the reaction suspension and the resulting solids were isolated by centrifugation. The purification of the Fe_3O_4/MnO hybrid nanocrystals was carried out by repeating the procedure including the dispersion in hexane, addition of acetone, and centrifugation processes three times.

Synthesis of Fe_3O_4HMON@*h*-SiO_2. Fe_3O_4/MnO dumbbell nanoparticles containing 12 nm sized Fe_3O_4 and 30 nm sized MnO components were synthesized by injecting 12 nm Fe_3O_4 nanocrystals into a solution containing 250 mg of $Mn(CH_3CO_2)_2$, 1.28 mg of oleic acid and 20 mL of trioctylamine. The silica coated dumbbell nanoparticles (Fe_3O_4/MnO@SiO_2) were prepared by a modified version of the previously reported reverse microemulsion technique. Polyoxyethylene(5)nonylphenyl ether (0.77 g, 1.74 mmol, Igepal CO-520, containing 50 mol % hydrophilic groups) was dispersed in a round-bottom flask containing cyclohexane solvent (17 mL). Next, a cyclohexane suspension (6 mL) of Fe_3O_4/MnO nanoparticles (6 mg) and an ammonium hydroxide solution (30%, 0.13 mL) were successively added with vigorous stirring to form a translucent suspension. Lastly, tetraethylorthosilicate (TEOS, 0.15 mL) was added and stirred for 12 h. The resulting Fe_3O_4/MnO@$SiO_2$was precipitated from the reaction suspension by the addition of methanol (1 mL) and retrieved by centrifugation. The crude Fe_3O_4/MnO@SiO_2s were purified by repeating the dispersion of the retrieved particles in ethanol and centrifugation several times. The purified Fe_3O_4/MnO@SiO_2 were redispersed in deionized water and stored for further use. For the synthesis of Fe_3O_4/HMON@*h*-SiO_2, 1 mg/mL of the Fe_3O_4/MnO@SiO_2 nanoparticles were treated with 1 M NH_2OH solution at room temperature for 72 h. The resulting Fe_3O_4/HMON@h-SiO_2 nanoparticles were isolated from the reaction suspension by centrifugation and purified by repeating the redispersion in water and centrifugation procedures.

General Procedure for Cyanosilylation Reactions Using Fe_3O_4/HMON@*h*-SiO_2 As a Catalyst. Fe_3O_4/HMON@*h*-SiO_2 catalyst (8 mol %, 0.040 mmol, based on Mn contents) dispersed in CH_2Cl_2 (2 mL) was treated with aryl aldehyde (0.5 mmol) and cyanotrimethylsilane (0.1 mL, 0.75 mmol) at 40 °C under an N_2 atmosphere. After stirring for 10 h, the catalyst was magnetically separated and the supernatant was concentrated to afford the product sample for ^{1}H NMR analysis. The conversion yields of the reactions were determined by ^{1}H NMR spectroscopy, and were calculated based on the following representative peaks of aldehyde (ArC*H*O, **1**) and cyanohydrins trimethylsilyl ether (ArC*H*CN(OTMS), **2**).^{1}H NMR (300 MHz, $CDCl_3$, δ): 10.01 (**1a**) and 5.49 (**2a**), 10.07 (**1b**) and 5.54 (**2b**), 10.42 (**1c**) and 6.06 (**2c**), 11.55 (**1d**) and 6.93 (**2d**), 10.41 (**1e**) and 5.72 (**2e**).

■ CONCLUDING REMARKS

In this study, we synthesized several Fe_3O_4/MnO hybrid nanocrystals through a seed-mediate growth process and found that the size of the seed nanocrystal is highly influential in determining the morphology of the resulting nanocrystal. In an application of the new hybrid nanocrystal synthesis methodology, we fabricated a novel nanocomposite containing a catalytically functionalized nanocavity, superparamagnetic nanocrystal, and porous, hollow shell. We also demonstrated the performance of this material as a nanoreactor that catalyzed the cyanosilylation reaction of aromatic aldehydes in a size selective manner and their ability to be recovered magnetically and reused without loss of catalytic activity even after ten successive cycles.

■ AUTHOR INFORMATION

Corresponding Author

*Tel: 82-54-279-2103. Fax: 82-54-279-3399. E-mail: insulee97@postech.ac.kr.

Notes

The authors declare no competing financial interest.

■ ACKNOWLEDGMENTS

This work was supported by the National Research foundation of Korea (KRF) grant funded by the Korea government (MEST) (2011-0017377).

■ REFERENCES

(1) Costi, R.; Saunders, A. E.; Banin, U. *Angew. Chem., Int. Ed.* **2010**, *49*, 4878−4897.
(2) Cozzoli, P. D.; Pellegrino, T.; Manna, L. *Chem. Soc. Rev.* **2006**, *35*, 1195−1208.
(3) Carbone, L.; Cozzoli, P. D. *Nano Today* **2010**, *5*, 449−493.
(4) Zeng, H.; Sun, S. *Adv. Funct. Mater.* **2008**, *18*, 391−400.
(5) Jun, Y.-w.; Choi, J.-s.; Cheon, J. *Chem. Commun.* **2007**, 1203−1214.
(6) Jiang, J.; Gu, H.; Shao, H.; Devlin, E.; Papaefthymiou, G. C.; Ying, J. Y. *Adv. Mater.* **2008**, *20*, 4403−4407.
(7) Xu, C.; Xie, J.; Ho, D.; Wang, C.; Kohler, N.; Walsh, E. G.; Morgan, J. R.; Chin, Y. E.; Sun, S. *Angew. Chem., Int. Ed.* **2008**, *47*, 173−176.
(8) Gu, H.; Yang, Z.; Gao, J.; Chang, C. K.; Xu, B. *J. Am. Chem. Soc.* **2005**, *127*, 34−35.
(9) Kwon, K.-W.; Shim, M. *J. Am. Chem. Soc.* **2005**, *127*, 10269−10275.
(10) Gao, J.; Zhang, W.; Huang, P.; Zhang, B.; Zhang, X.; Xu, B. *J. Am. Chem. Soc.* **2008**, *130*, 3710−3711.
(11) Shi, W.; Zeng, H.; Sahoo, Y.; Ohulchanskyy, T. Y.; Ding, Y.; Wang, Z. L.; Swihart, M.; Prasad, P. N. *Nano Lett.* **2006**, *6*, 875−881.
(12) Figuerola, A.; Fiore, A.; Corato, R. D.; Falqui, A.; Giannini, C.; Micotti, E.; Lascialfari, A.; Corti, M.; Cingolani, R.; Pellegrino, T.; Cozzoli, P. D.; Manna, L. *J. Am. Chem. Soc.* **2008**, *130*, 1477−1487.
(13) Buonsanti, R.; Grillo, V.; Carlino, E.; Giannini, C.; Gozzo, F.; Garcia.-Hernandez, M.; Garcia, M. A.; Cingolani, R.; Cozzoli, P. D. *J. Am. Chem. Soc.* **2010**, *132*, 2437−2464.
(14) Yang, J.; Peng, J.; Zhang, Q.; Peng, F.; Wang, H.; Yu, H. *Angew. Chem., Int. Ed.* **2009**, *48*, 3991−3995.
(15) Pang, M.; Hu, J.; Zeng, H. C. *J. Am. Chem. Soc.* **2010**, *132*, 10771−10785.
(16) Pan, Y.; Gao, J.; Zhang, B.; Zhang, X.; Xu, B. *Langmuir* **2010**, *26*, 4184−4187.
(17) Anisur, R. M.; Shin, J.; Choi, H. H.; Yeo, K. M.; Kang, E. J.; Lee, I. S. *J. Mater. Chem.* **2010**, *20*, 10615−10621.
(18) Yin, M.; O'Brien, S. *J. Am. Chem. Soc.* **2003**, *125*, 10180−10181.
(19) Masala, O.; Seshadri, R. *J. Am. Chem. Soc.* **2005**, *127*, 9354−9355.
(20) Leff, D. V.; Ohara, P. C.; Heath, J. R.; Gelbart, W. M. *J. Phys. Chem.* **1995**, *99*, 7036−7041.
(21) Talapin, D. V.; Rogach, A. L.; Haase, M.; Weller, H. *J. Phys. Chem. B* **2001**, *105*, 12278−12285.

(22) Dabbousi, B. O.; Rodriguez-Viejo, J.; Mikulec, F. V.; Heine, J. R.; Mattoussi, H.; Ober, R.; Jensen, K. F.; Bawendi, M. G. *J. Phys. Chem. B* **1997**, *101*, 9463−9475.
(23) Mokari, T.; Rothenberg, E.; Popov, I.; Costi, R.; Banin, U. *Science* **2004**, *304*, 1787−1790.
(24) Lee, J.-S.; Bodnarchuk, M. I.; Shevchenko, E. V.; Talapin, D. V. *J. Am. Chem. Soc.* **2010**, *132*, 6382−6391.
(25) McDaniel, H.; Shim, M. *ACS Nano* **2009**, *3*, 434−440.
(26) Pellegrino, T.; Fiore, A.; Carlino, E.; Giannini, C.; Cozzoli, P. D.; Ciccarella, G.; Respaud, M.; Palmirotta, L.; Cingolani, R.; Manna, L. *J. Am. Chem. Soc.* **2006**, *128*, 6690−6698.
(27) Shylesh, S.; Schünemann, V.; Thiel, W. R. *Angew. Chem., Int. Ed.* **2010**, *49*, 3428−3459.
(28) Polshettiwar, V.; Varma, R. S. *Green Chem.* **2010**, *12*, 743−754.
(29) Lim, C. W.; Lee, I. S. *Nano Today* **2010**, *5*, 412−434.
(30) Jun, C.-H.; Park, Y. J.; Yeon, Y.-R.; Choi, J.-r.; Lee, W.-r.; Ko, S.-j.; Cheon, J. *Chem. Commun.* **2006**, 1619−1621.
(31) Amali, A. J.; Rana, R. K. *Green Chem.* **2009**, *11*, 1781−1786.
(32) Lin, F.-h.; Doong, R.-a. *J. Phys. Chem. C* **2011**, *115*, 6591−6598.
(33) Mori, K.; Kondo., Y.; Yamashita, H. *Phys. Chem. Chem. Phys.* **2009**, *11*, 8949−8954.
(34) Horike, S.; Dincă, M.; Tamaki, K.; Long, J. R. *J. Am. Chem. Soc.* **2008**, *130*, 5854−5855.
(35) Ikeda, S.; Kobayashi, H.; Ikoma, Y.; Harada, T.; Torimoto, T.; Ohtani, B.; Matsumura, M. *Phys. Chem. Chem. Phys.* **2007**, *9*, 6319−6326.
(36) Park, J.; An, K.; Hwang, Y.; Park, J.-G.; Noh, H.-J.; Kim, J.-Y.; Park, J.-H.; Hwang, N.-M.; Hyeon, T. *Nat. Mater.* **2004**, *3*, 891−895.